SPIE Proceedings, *Ophthalmic Technologies XV*, vol. 5688A, 2005

Optical monitoring of thermal effects in RPE during heating

G. Schuele[1,2], Ph. Huie[1,2], D. Yellachich[1], F. Molnar[1],
C. O'Conell-Rodwell[3], E. Vitkin[4], L. T. Perelman[5], D. Palanker[1,2]

[1]Department of Ophthalmology, [2]Hansen Experimental Physics Laboratory, [3]Department of Pediatrics, Microbiology & Immunology and Radiology, Stanford University, CA 94305, USA
[4]Biomedical Imaging and Spectroscopy Laboratory, Beth Israel Deaconess Medical Center, Harvard Medical School, MA 02215, USA

ABSTRACT

Fast and non-invasive detection of cellular stress is useful for fundamental research and practical applications in medicine and biology. Using Light Scattering Spectroscopy we extract information about changes in refractive index and size of the cellular organelles. Particle sizes down to 50nm in diameter can be detected using light within the spectral range of 450-850 nm. We monitor the heat-induced sub-cellular structural changes in human RPE cells and, for comparison, in transfected NIH-3T3 cells which express luciferase linked to the heat shock protein (HSP). Using inverse light scattering fitting algorithm, we reconstruct the size distribution of the sub-micron organelles from the light scattering spectrum. The most significant (up to 70%) and rapid (20sec) temperature-related changes can be linked to an increase of refractive index of the 160nm sized mitochondria. The start of this effect coincides with the onset of HSP expression. This technique provides an insight into metabolic processes within organelles larger than 50nm without exogenous staining and opens doors for non-invasive real-time assessment of cellular stress, which can be used for monitoring of retinal laser treatments like transpupillary thermo therapy or PDT.

Keywords: thermal stress, online dosimetry, light scattering spectroscopy, heat shock protein

1. INTRODUCTION

Transformations of the organelles under conditions of cellular stress are known very little because of their small sizes and low optical contrast. Multiphoton imaging techniques[1] can resolve subcellular structures but require staining to improve the contrast, which often affects cellular metabolism[2]. Electron microscopy provides high resolution but is incompatible with imaging of live cells. Recently, Light Scattering Spectroscopy (LSS)[3] was introduced for non-invasive sizing of organelles in large populations of cells[4].

The metabolic responses of cells to various stress factors are of great interest to biology and medicine and have been extensively studied. One of the best known responses of cells to stress is the expression of heat shock proteins (HSP)[5]. The HSP expression after thermal stress is the metabolic reaction induced by misaggregation and denaturation of proteins, changes in membrane permeability and disruption of cytoskeletal components[6]. Initial expression of the heat shock factors (HSF)[7] regulates the HSP expression which peaks several hours after the thermal shock[8]. To the best of our knowledge, there is no non-invasive technique for detection or monitoring of cellular metabolism and associated changes in organelles occurring during and after cellular stress.

Cellular organelles and cell boundaries scatter light with angular and spectral characteristics dependent on the sizes and relative refractive indexes of the scattering particles. With LSS these parameters can be extracted from the scattering spectrum collected at well-defined angles[3, 4]. Information about sizes and density of the scattering particles obtained from the scattering spectra can be used for fast and non-invasive monitoring of the metabolic transformations in cells under stress[9].

Using LSS we study the reaction of the retinal pigment epithelial (RPE) cells to thermal stress. Motivation for this study comes from the fact that melanosomes within the RPE cells strongly absorb light[10] and thus the RPE is the hottest layer of cells during laser treatments of the retina[11]. In retinal laser therapies involving prolonged heating, such as Transpupillary Thermal Therapy (TTT) [12], the temperature rise in the retina strongly varies from patient to patient due to variation in pigmentation and blood perfusion. Strong differences in temperature result in large variability and poor predictability of the clinical outcomes.

In preliminary experiments[9] with mixtures of polystyrene beads we could show that LSS allows sizing down to 50nm with 10nm precision. Also the correct relative concentration ratio of a polystyrene bead mixture was determined.

2. MATERIAL AND METHODS

2.1. Setup

A sketch of the setup is shown in Figure 1. Light from a broadband halogen lamp was coupled into a 3mm fiber bundle. The fiber tip was imaged 1:1 through a 50% beamsplitter onto a sample illuminating approximately 10000 RPE cells within a 3 mm spot. The back-scattered (180 ± 5 deg.) light from the sample passing through the 50% beamsplitter was directed via an upright microscope (Leica, MZ16) into an optical multichannel analyzer (Ocean Optics, USB2000). A spectrum ranging from 350nm to 900nm and containing 2048 points was typically acquired during 2 seconds. The sample chamber was placed on a black light absorbing glass (OD5) with glycerin as an index matching material. To avoid specular reflections from the sample chamber, the whole sample mount was tilted off the optical axis by several degrees.

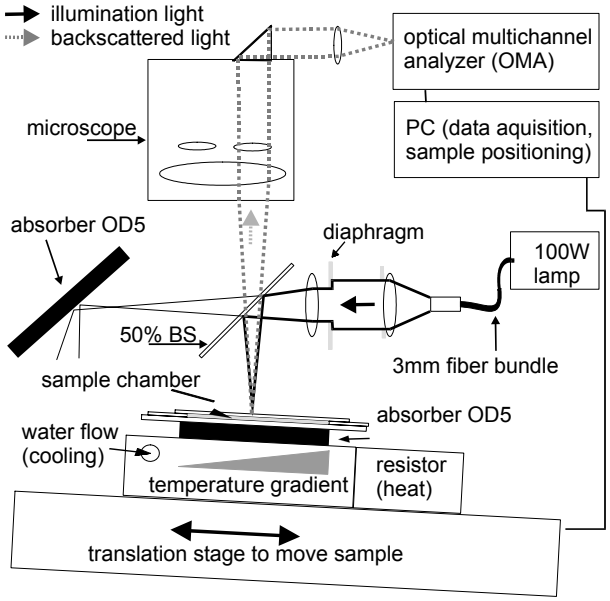

Figure 1. Light scattering spectroscopy setup for the detection of temperature induced cellular stress.

The sample mount was heated on one and cooled on the other side to produce a temperature gradient of about 10°C over 5cm of distance across the sample. Temperature-time courses for different locations in the sample chamber were measured with a micro thermocouple. To measure cellular responses at different temperature courses within the sample the whole mount was moved under the stationary optical setup using a stepper motor. The scattering spectra were acquired every 10 seconds. The setup was controlled by LabView (National Instruments, 6.1) on PC.

2.2. Sample preparation and experiments

For detection of the thermal stress in cells the human RPE cell line ATCC and the NIH-3T3 cells were confluently grown on glass slides. The NIH-3T3 cells were transfected with a light-emitting luciferus gene linked to HSP[8]. The HSP expression from these cells can be detected by imaging (IVIS, Xenogen Corp., Alameda, CA, USA) the luminescence due to the luciferase activity. During the measurements the cells were covered with phosphate buffered solution to avoid light absorption within the colored cell medium, and the sample was covered with a cover slide. To study the reaction of organelles to thermal stress the sample slides were placed on a mount with a temperature gradient ranging from 40°C to 50°C. The mount was heated for 15 minutes and then cooled down to room temperature. The scattering spectra were measured in 5 locations on the slides corresponding to 5 different temperatures within this range. After the experiments all cells were alive as indicated by the live/dead calceinAM and edithium homodimer fluorescent assay[13].

To verify precision in assessment of the organelle sizes based on their scattering spectrum the light scattering spectrum of RPE cells was measured and the data were analyzed by the inverse light scattering fitting algorithm (see Sec. 2.3). To compare the extracted LSS based organelle size distribution a transmission electron microscopy (TEM) histological study was performed. For the TEM study RPE cells were grown on a mylar film. After fixation with 2.5% glutaraldeyhde / 1% paraformaldehyde, embedding in LX-112 and staining in uranyl acetate / lead citrate, the 200 nm-thick sections were examined under a TEM. The distribution of sizes of different organelles in the TEM photographs were analyzed using the ImageJ software[14].

2.3. Inverse light scattering fitting algorithm

In a single scattering approximation the scatterer size density distributions $N(D)$ were extracted from the measured scattering spectra using the following Mie theory-based approach. If incident light is scattered by the particles of various diameters D, the scattered light intensity can be expressed as an integral over all diameters:

$$I = I_0 C \int N(D) dD \int_0^{\theta_0} \int_0^{2\pi} \sin\theta_i d\theta_i d\varphi_i \int_0^{\theta_0} \int_0^{2\pi} \sin\theta_s d\theta_s d\varphi_s \left(\left| S_1(\theta, n, D, \lambda) \right|^2 + \left| S_2(\theta, n, D, \lambda) \right|^2 \right), \quad (1)$$

where I_0 is the intensity of the incident wave, C is the apparatus constant of the system, θ_0 is the delivery/collection angle of the system, θ is the scattering angle which depends on the angles of incoming light θ_i, φ_i and the angles of the scattered light θ_s, φ_s, and $S_1(\theta, n, D, \lambda)$ and $S_2(\theta, n, D, \lambda)$ are diagonal elements of the scattering matrix at given wavelength λ and relative refractive index $n = n_s / n_0$, where n_s is the refractive index of the scatterer and n_0 is the refractive index of the surrounding medium. The elements of the scattering matrix are calculated using Mie theory[15].

Expression (1) relates the intensity spectrum of scattered light $I(\theta, n, D, \lambda)$ to the scattering amplitudes $S_1(\theta, n, D, \lambda)$ and $S_2(\theta, n, D, \lambda)$. In backscattering direction, the spectrum $I(\theta, n, D, \lambda)$ of a submicron particle with the relative refractive index close to unity has unique modulations, which depend on the scatterer diameter D and scales proportionally to $(n-1)^2$. The light scattering spectra of particles smaller than 50 nm are featureless and the Mie theory approximates to a classical Rayleigh scattering[16]. The scatterer size density distribution $N(D)$ for sizes larger than 50nm can thus be extracted by fitting[17] the predictions of the model to the measured scattering spectrum. We have developed such automated inversion procedure, which extracts the size density histogram of the scatterers that best fit the measured light scattering spectrum[4]. The relative refractive index of sub-cellular organelles used for these calculations was $n = 1.04$[18] and for the polystyrene beads $n = 1.20$. The code is written in Fortran and runs reasonably fast (~10 seconds per spectrum) on a conventional PC (Pentium, 2GHz, Windows OS).

3. RESULTS AND DISCUSSION

3.1. Sizing of cellular organelles

To validate the LSS assessment of the sizes of cellular organelles, the light scattering spectrum of RPE cells was measured at 37°C (Figure 2A), and the scatterer density histogram was extracted from this spectrum using the inverse light scattering algorithm (Sec. 2.3). This histogram was then compared to the size distribution extracted from a series of 200 nm-thick histological sections of these cells photographed on TEM (Figure 2B). To make the results of LSS comparable to the size distribution observed in histological sections, the scatterer density histogram was converted into a histogram representing a statistical distribution of cross-sections of organelles in the arbitrary oriented sections of 200nm in thickness (Figure 2B). Both, the LSS-based and the histology–based histograms have two distinct peaks at 140nm and 360nm. Conversion of the histograms corresponding to 3-dimentional particles into the distribution of diameters in the 2-dimentional slices resulted in a slight shift of their maxima: the actual sizes of the organelles have slightly bigger mean diameters: 160nm and 385nm. The smaller size peak appears to be the cross-sectional diameter of

mitochondria and the bigger particles represent such organelles as multivesicular granules, membrane-bound granules and dense granules.

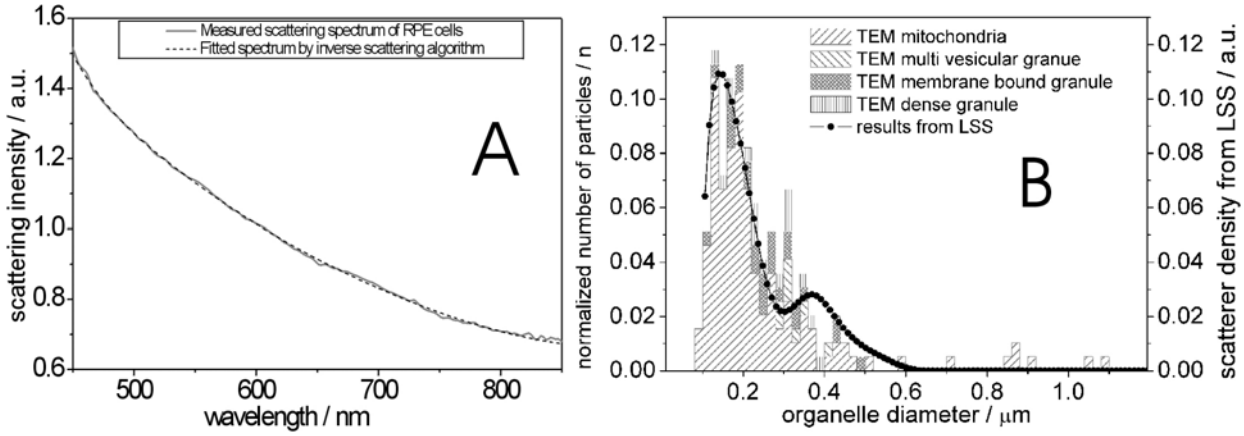

Figure 2A. Light scattering spectrum of RPE cells and the spectrum fitted with the inverse light scattering algorithm. **B.** The size histogram of the RPE organelles extracted from the scattering spectrum and the histogram measured in histological sections using TEM. The scatterer density represents a product of $(n-1)^2$ and the number of organelles (n is the relative refractive index). The 140nm peak in the histogram corresponds to the width of mitochondria. The second (360nm) peak corresponds to multivesicular bodies, membrane bound granules and dense granules.

Good correspondence of the organelle size distribution extracted from the light scattering spectrum to the results of the TEM study shown in Figure 2B demonstrates precision of our inverse light scattering algorithm. For cellular organelles, which are generally are not spherical, the agreement of the extracted scatterer density histogram with the TEM analysis supports the validity of the spherical approximation for this type of scatterers.

3.2. Optical detection of cellular stress

In experiments with cells the spectral changes appeared within one minute after the onset of heating. The heat-induced changes in the scattering spectra (Figure 3A) were more pronounced in the long wavelength region. The scatterer density histograms (Figure 3B) extracted from the measured spectra (shown in Figure 3A) demonstrate that the scattering density of the 160nm mitochondria increased very significantly (up to 50%) and the distribution slightly shifts (up to 15nm) towards the bigger sizes. The second peak at 385nm does not change significantly. The scatterer density in the histogram represents a product of the $(n-1)^2$ (where n is a relative refractive index of the particle) and the number of particles [4], thus an increase in the scatterer density reflects the increase in the refractive index of the organelle.

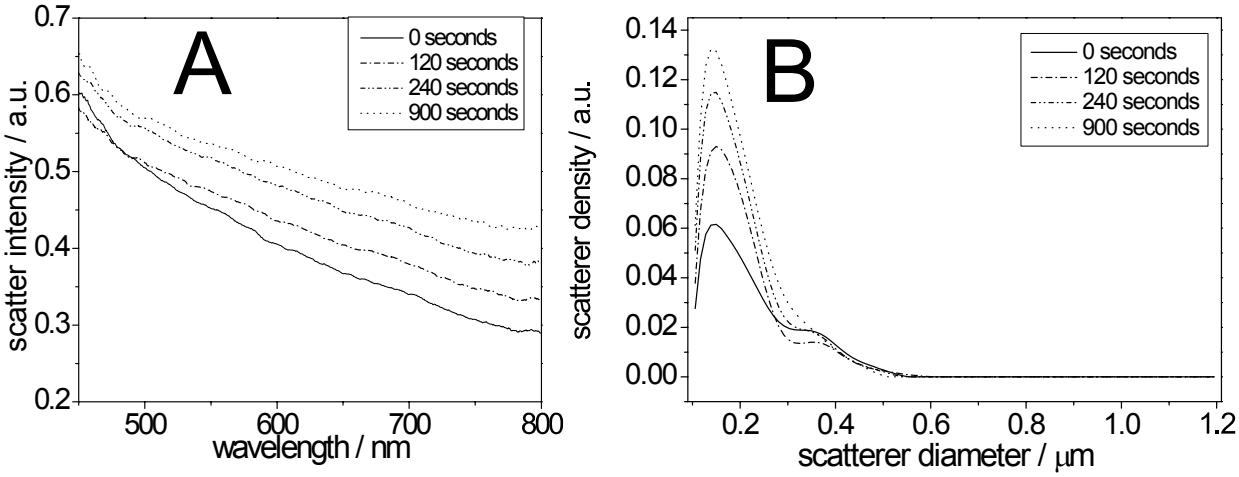

Figure 3A. Light scattering spectra of the RPE cells at different moments of time under thermal stress of 47.5 °C. The temperature-induced spectral changes are more pronounced in the long wavelength region. **B**. Corresponding histograms of the scatterer density extracted from the spectra. Amplitude of the 160nm peak in the histogram strongly increases during heating, while its position slightly shifts towards larger sizes. Increase in the amplitude represents the rise of the refractive index of the organelles probably due to the enhanced metabolic activity.

Figure 4A shows the time course of the maximum scattering density for different temperatures. It starts increasing at 42.5°C and shows a much stronger response at 45.0°C. The onset of this effect is earlier and stronger at higher temperatures. However, for the highest temperature of 50°C the scattering density increase is smaller than at 47.5°C, which probably indicates that metabolic response decreases at these high temperatures. Starting at temperatures of 47.5°C, the density peak shifts up to 15nm towards bigger sizes (Figure 4B) and the width of the distribution increases (not shown). Both of these effects become most pronounced at the highest temperature of 50.0°C. All cells were still viable after the heating as proved by the live/dead fluorescent assay [13].

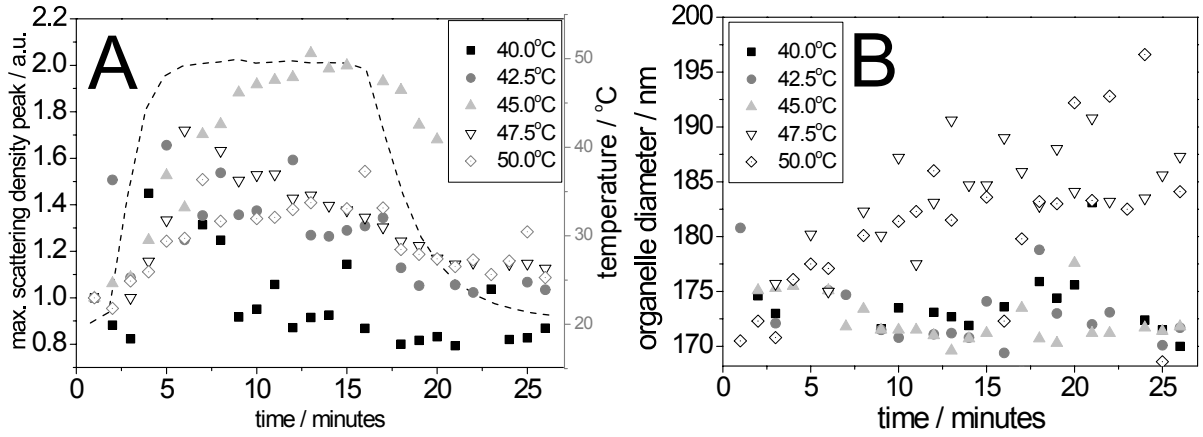

Figure 4A Time course of the maximum scatterer density (i.e. relative refractive index) of the RPE organelles at different maximal temperatures. The temperature course of the 50.0°C point on the sample is plotted as a line, with the temperature scale on the right. A slight increase of the scattering density can be seen for 42.5°C, and it reaches its maximum at 45.0°C. The increase starts earlier at higher temperatures. Interestingly, at 50°C the increase in scattering density is less pronounced than at 47.5°C and 45.0°C, indicating that metabolic response is suppressed. **B** The width of the mitochondria increase with time by about 15nm at temperatures of 47.5°C - 50.0°C.

To confirm our findings regarding metabolic response of organelles at different temperatures we studied expression of the heat shock protein (HSP) in the NIH-3T3 cells under the same experimental conditions. The extracted scatterer density histograms of the NIH-3T3 cells were similar to the histograms obtained with the RPE cells (shown in Figure 2B). Figure 5A shows the temporal course of the scattering density at the 160nm position of the peak. The time course of the actual temperature on a sample in a position corresponding to the maximal temperature of 45°C is shown with a red dashed line. As one can see in Figure 5A, significant increase in the scatterer density starts at 41°C and intensifies at higher temperatures. The cellular response is delayed with respect to the onset of heating, and this delay decreases at higher temperatures. Figure 5B shows the expression of HSP on the sample slide 6 hours after heating, which was measured by light emission induced by the luciferase linked to HSP. Peak of the HSP expression was observed at 43°C, which is in a good agreement with the previously published data [8]. No size shift of the maximum scattering density or broadening of the distribution was found with NIH-3T3 cells.

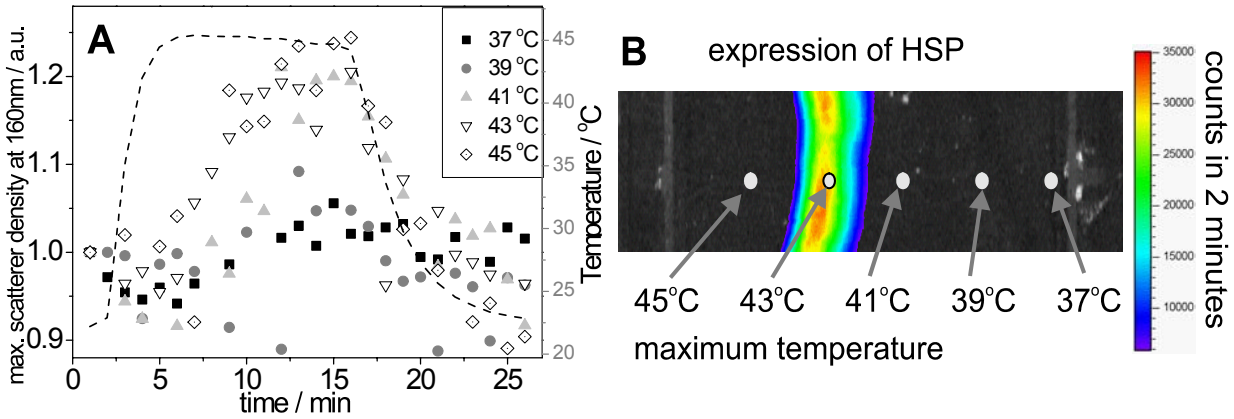

Figure 5A. Time course of the scatterer density of the 160nm organelles for different maximal temperatures in the NIH-3T3 cells. The time course of the 45°C point is plotted with a dashed line (temperature scale on the right). Significant increase of the scattering density starts at 41°C. The onset of this effect is earlier at higher temperatures. No significant changes of the scatterer sizes have been observed at these temperatures. **B**. Expression of HSP measured by light emission of luciferase 6 hours after the exposure. The red dots mark the areas with different temperatures where the scattering spectra were acquired. The HSP expression peaks at 43°C.

4. CONCLUSION

This study demonstrates that LSS can be successfully used for rapid and non-invasive monitoring of the early subcellular transformations in living cells under thermal stress. The light scattering properties of cells are known to change during cell proliferation[19], apoptosis[20], toxic stress[21, 22] and osmotic shock[23]. With LSS, the subcellular origin and the specific organelles associated with these effects can now be identified and monitored in real time. This technique can be applied to organelles with dimensions down to 50 nm, and opens doors to quantitative real-time assessment of the organelle reactions to various types of cellular stress without exogenous staining or labeling.

As LSS is a pure optical technique it can be used for non-invasive monitoring of therapies. Future work will show if LSS will allow for monitoring the subthreshold laser lesions during retinal treatments with TTT or PDT.

1. S. W. Hell, *Toward fluorescence nanoscopy.* Nat Biotechnol, 2003. **21**(11): p. 1347-55.
2. W. T. Mason, *Fluorescent and Luminescent Probes for Biological Activity*. 1999: Academic Press.
3. L. T. Perelman, V. Backman, M. Wallace, G. Zonios, R. Manoharan, A. Nusrat, S. Shields, M. Seiler, C. Lima, T. Hamano, I. Itzkan, J. Van Dam, J. M. Crawford, and M. S. Feld, *Observation of periodic fine structure in reflectance from biological tissue: a new technique for measuring nuclear size distribution.* Physical Review Letters, 1998. **80**(3): p. 627-30.

4. H. Fang, M. Ollero, E. Vitkin, L. M. Kimerer, P. B. Cipolloni, M. M. Zaman, S. D. Freedman, I. J. Bigio, I. Itzkan, E. B. Hanlon, and L. T. Perelman, *Noninvasive sizing of subcellular organelles with light scattering spectroscopy.* IEEE Journal of Selected Topics in Quantum Electronics, 2003. **9**(2): p. 267-76.
5. J. G. Kiang, G. C. Tsokos, *Heat shock protein 70 kDa: molecular biology, biochemistry, and physiology.* Pharmacol Ther, 1998. **80**(2): p. 183-201.
6. L. A. Sonna, J. Fujita, S. L. Gaffin, C. M. Lilly, *Invited review: Effects of heat and cold stress on mammalian gene expression.* J Appl Physiol, 2002. **92**(4): p. 1725-42.
7. L. Pirkkala, P. Nykanen, L. Sistonen, *Roles of the heat shock transcription factors in regulation of the heat shock response and beyond.* Faseb J, 2001. **15**(7): p. 1118-31.
8. C. E. O'Connell-Rodwell, D. Shriver, D. M. Simanovskii, C. McClure, Y. A. Cao, W. Zhang, M. H. Bachmann, J. T. Beckham, E. D. Jansen, D. Palanker, H. A. Schwettman, and C. H. Contag, *A genetic reporter of thermal stress defines physiologic zones over a defined temperature range.* Faseb J, 2004. **18**(2): p. 264-71.
9. G. Schuele, P. Huie, A. Vankov, E. Vitkin, F. Hui, E. B. Hanlon, L. T. Perelman, and D. Palanker, *Noninvasive monitoring of the thermal stress in RPE using light scattering spectroscopy.* Proc. SPIE, 2004. **5314**: p. 95-99.
10. *Laser photocoagulation of subfoveal recurrent neovascular lesions in age-related macular degeneration. Results of a randomized clinical trial. Macular Photocoagulation Study Group.* Archives of Ophthalmology, 1991. **109**(9): p. 1232-1241.
11. M. A. Mainster, T. J. White, J. H. Tips, P. W. Wilson, *Retinal-temperature increases produced by intense light sources.* J Opt Soc Am, 1970. **60**(2): p. 264-70.
12. M. A. Mainster, E. Reichel, *Transpupillary thermotherapy for age-related macular degeneration: long-pulse photocoagulation, apoptosis, and heat shock proteins.* Ophthalmic Surg Lasers, 2000. **31**(5): p. 359-373.
13. Molecular, Probes, *LIVE/DEAD Viability/Cytotoxicity, Product Information.* 2001.
14. W. Rusband, *ImageJ 1.32*. 2004, National Institute of Health.
15. G. Mie, *Beitraege zur Optik trueber Medien, speziell kolloidaler Metalloesungen.* Ann. Phys., 1908. **29**: p. 377-445.
16. C. F. Bohren, D. R. Huffman, *Absorption and Scattering of Light by Small Particles*. 1998, New York: Wiley.
17. IMSL, *DLCLSQ : Linear least-square problems with linear constrains*, in *DLCLSQ : Linear least-square problems with linear constrains*. 2003, Visual Numerics IMSL: San Ramon.
18. L. T. Perelman, V. Backman, *Light scattering spectroscopy of epithelial tisuues: Principles and applications*, in *Handbook on Optical Biomedical Diagnostics*, V. Tuchin, Editor. 2002, SPIE: Bellingham. p. 675-724.
19. J. R. Mourant, M. Canpolat, C. Brocker, O. Esponda-Ramos, T. M. Johnson, A. Matanock, K. Stetter, and J. P. Freyer, *Light scattering from cells: the contribution of the nucleus and the effects of proliferative status.* J Biomed Opt, 2000. **5**(2): p. 131-7.
20. Z. Shiffer, N. Zurgil, Y. Shafran, M. Deutsch, *Analysis of laser scattering pattern as an early measure of apoptosis.* Biochem Biophys Res Commun, 2001. **289**(5): p. 1320-7.
21. D. N. Georgieva, N. Genov, K. Hristov, K. Dierks, C. Betzel, *Interactions of the neurotoxin vipoxin in solution studied by dynamic light scattering.* Biophys J, 2004. **86**(1 Pt 1): p. 461-6.
22. B. V. Bronk, Z. Z. Li, J. Czege, *Polarized light scattering as a rapid and sensitive assay for metal toxicity to bacteria.* J Appl Toxicol, 2001. **21**(2): p. 107-13.
23. S. P. Srinivas, J. A. Bonanno, E. Lariviere, D. Jans, W. Van Driessche, *Measurement of rapid changes in cell volume by forward light scattering.* Pflugers Arch, 2003.